

Disorder driven spin-orbital liquid behaviour in the $\text{Ba}_3\text{XSb}_2\text{O}_9$ materials

Andrew Smerald¹ and Frédéric Mila¹

¹*Institut de Théorie des Phénomènes Physiques, Ecole Polytechnique Fédérale de Lausanne (EPFL), CH-1015 Lausanne, Switzerland*

(Dated: December 3, 2024)

Recent experiments on the $\text{Ba}_3\text{XSb}_2\text{O}_9$ family have revealed materials that potentially realise spin- and spin-orbital liquid physics. However, the lattice structure of these materials is complicated due to the presence of charged X^{2+} - Sb^{5+} dumbbells, with two possible orientations. To model the lattice structure, we consider a frustrated model of charged dumbbells on the triangular lattice, with long-range Coulomb interactions. We study this model using Monte Carlo simulation, and find a freezing temperature, T_{frz} , at which the simulated structure factor matches well to low-temperature x-ray diffraction data for $\text{Ba}_3\text{CuSb}_2\text{O}_9$. At $T = T_{\text{frz}}$ we find a complicated “branching” structure of superexchange-linked X^{2+} clusters, and show that this gives a natural explanation for the presence of orphan spins. Finally we provide a plausible mechanism by which such dumbbell disorder can promote a spin-orbital resonant state with delocalised orphan spins.

PACS numbers: 75.10.Kt, 75.25.Dk, 75.47.Lx

Recently there has been an intense search for materials exhibiting spin-liquid behaviour – materials beyond the “standard model” of condensed matter physics¹. A particularly intriguing idea is of a spin-orbital liquid, in which not only the spin but also the orbital degrees of freedom remain fluctuating down to low temperature^{1–5}.

The $\text{Ba}_3\text{XSb}_2\text{O}_9$ family, with $\text{X}=\text{Cu}^{6–15}, \text{Ni}^{16–20}, \text{Co}^{21–23}, \text{Mn}^{24,25} \dots$, has been shown to be a promising class of materials to realise spin-liquid behaviour. $\text{Ba}_3\text{CuSb}_2\text{O}_9$ has been particularly well studied, and it has been suggested that the spin and orbital degrees of freedom associated with the Cu^{2+} ions form a spin-orbital liquid state^{6–15}. In the case of $\text{Ba}_3\text{NiSb}_2\text{O}_9$, the pressure-synthesised 6H-B structure has been proposed as an example of a spin-1 spin-liquid state^{16–20}.

An important starting point when trying to understand spin-liquid behaviour is knowledge of the lattice structure. In $\text{Ba}_3\text{CuSb}_2\text{O}_9$ it has been suggested that the Cu^{2+} ions form a short-range honeycomb lattice⁷, and theoretical approaches have therefore concentrated on Cu^{2+} plaquettes formed of several hexagons^{10,12,15}. On the other hand, in the 6H-B phase of $\text{Ba}_3\text{NiSb}_2\text{O}_9$ it has been suggested that the Ni^{2+} ions form a triangular lattice¹⁶.

Here we argue that in neither case is this a good starting point for theoretical investigation, and instead one should consider a disordered “branch” lattice [see Fig. 1b]. The evidence we present focuses in particular on $\text{Ba}_3\text{CuSb}_2\text{O}_9$, but should be applicable to other members of the $\text{Ba}_3\text{XSb}_2\text{O}_9$ family. Furthermore, we suggest that this type of correlated lattice disorder can promote spin-orbital liquid behaviour.

In order to investigate the lattice structure of these materials, we solve a frustrated model of interacting X^{2+} - Sb^{5+} charged dumbbells [see Fig. 1]. We argue this is relevant to stoichiometric $\text{X}=\text{Cu}$, $\text{X}=\text{Ni}$ in the pressure synthesised 6H-B phase and potentially to pressure synthesised $\text{X}=\text{Mn}$ and $\text{X}=\text{Co}$.

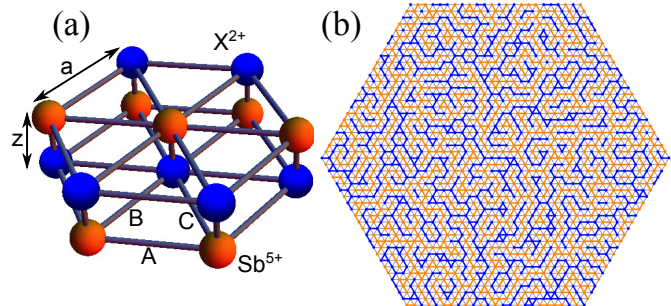


FIG. 1: Charged dumbbells on the triangular lattice. (a) X^{2+} - Sb^{5+} dumbbells of length z form a triangular lattice bilayer, with lattice constant a . There is an Ising degree of freedom associated to whether the dumbbell is orientated with X above Sb or vice versa. The equilibrium distribution of dumbbells can be mapped onto a charge model, E_{Coul} [Eq. 1], which at low temperature orders in a stripe ground state, with stripes parallel to A (shown here) B or C bonds. (b) Material realisations of E_{Coul} [Eq. 1] fall out of equilibrium at $T = T_{\text{frz}}$, and the lattice structure can be studied by making simulations at this temperature. A snapshot of a typical lattice structure for $\text{X}=\text{Cu}$ is shown, with blue and orange sites denoting different dumbbell orientations. Superexchange interactions link Cu^{2+} ions on dumbbells with the same orientation, and superexchange linked clusters are shown by blue and orange bonds.

The X^{2+} - Sb^{5+} dumbbells are surrounded by O^{2-} biocatahedra, and their constituent ions sit on the vertices of stacked triangular lattice bilayers⁷, as shown in Fig. 1a. Each dumbbell has two possible orientations with either the X^{2+} or Sb^{5+} on top. Electrostatically, the primary influence on the orientation of the dumbbells is the orientation of the other dumbbells – that is to say that the Ba^{2+} , O^{2-} and remaining Sb^{5+} ions are electrostatically ambivalent as to the dumbbell orientation.

This leads us to consider a Coulombic charge model,

$$E_{\text{Coul}} = \frac{1}{2} \sum_{i \neq j} \frac{q_i q_j}{r_{ij}}, \quad (1)$$

where $q_i = \pm 1$ is a normalised charge, i and j run over

the sites of a bilayer triangular lattice [shown in Fig. 1], $r_{ij} = |\mathbf{r}_i - \mathbf{r}_j|$ and the charge distribution is constrained to have one positive and one negative charge on each dumbbell. We ignore interaction between dumbbells in different bilayers, and we provide an *a posteriori* justification for this approximation.

In order to relate the charge distribution following from E_{Coul} [Eq. 1] to the lattice structure of the materials, it is necessary to understand the synthesis process. This is typically performed at high temperature ($>1000^{\circ}\text{C}$), and the crystals are then slowly cooled to room temperature and below^{7,8}. A characteristic timescale t_{cool} can be ascribed to this cooling process, and this should be compared to t_{flip} , the characteristic time for dumbbells to reverse their orientation. Close to the synthesis temperature, we assume that $t_{\text{flip}} \ll t_{\text{cool}}$, and therefore the dumbbell orientation remains in thermal equilibrium as T is reduced. As the crystal is cooled, t_{flip} increases, and there is a temperature, T_{frz} , below which $t_{\text{flip}} \gg t_{\text{cool}}$. In this regime the dumbbell dynamics is too slow to equilibriate the system and the charge distribution is thus frozen in place. The dumbbell structure for any $T < T_{\text{frz}}$ can therefore be understood from studying the equilibrium dumbbell structure at $T = T_{\text{frz}}$.

One piece of evidence that the dumbbells are dynamic at high temperature comes from the isostructural compound $\text{Ba}_3\text{IrTi}_2\text{O}_9$ ²⁶. Here the Ir-Ti dumbbells exhibit a markedly different low-temperature structure depending on whether the material is slowly cooled from the synthesis temperature (1000°C) or quenched. Also, the dumbbells in these materials are quite widely spaced – there is no sharing of neighbouring O^{2-} ions – and thus it seems reasonable that they should be flippable at high temperature.

This suggests a twofold strategy for understanding the lattice structure of these materials. 1) Simulate E_{Coul} [Eq. 1] as a function of temperature, and, by comparison with experimental data, determine the freezing temperature, T_{frz} . 2) Simulate the model at T_{frz} in order to extract detailed information about the lattice structure for all $T < T_{\text{frz}}$.

In order to simulate E_{Coul} [Eq. 1], it is first mapped onto an Ising model on the triangular lattice using Ewald summation²⁷. This leads to,

$$E_{\text{Coul}} = E_0 + \frac{1}{2} \sum_{i,j} \psi_{ij}(z) \sigma_i \sigma_j, \quad (2)$$

where $\sigma_i = \pm 1$ is an Ising spin, i runs over the sites of a triangular lattice and $\psi_{ij}(z)$ defines the interactions between sites as a function of the dumbbell size, z [see Fig. 1]. For $z \rightarrow 0$, E_{Coul} [Eq. 2] reduces to interacting Ising dipoles on the triangular lattice²⁸. Here we consider $z = 0.46a$ as this is relevant to $\text{Ba}_3\text{CuSb}_2\text{O}_9$.

We have performed Monte Carlo simulations of E_{Coul} [Eq. 2] over a wide range of temperatures. Here we provide a brief account of the low temperature phase transition, postponing a detailed description to another publication.

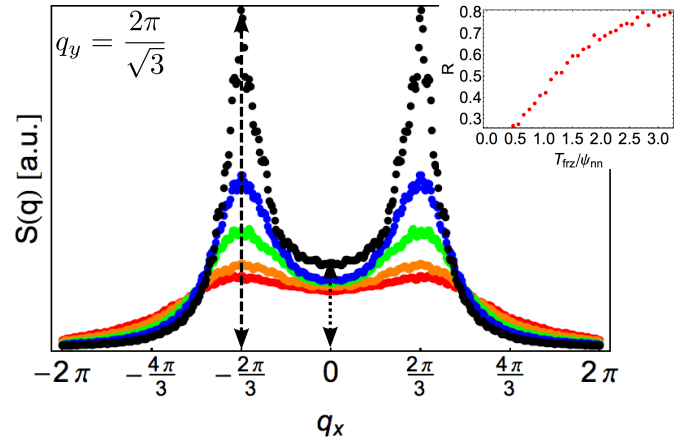


FIG. 2: The dumbbell structure factor, $S(\mathbf{q})$, as predicted by simulations of E_{Coul} [Eq. 1]. The structure factor is plotted at a range of temperatures as a function of q_x with $q_y = 2\pi/\sqrt{3}$ and $q_z = \pi$. From top to bottom: $T/\psi_{\text{nn}} = 0.45$ (black), $T/\psi_{\text{nn}} = 0.9$ (blue), $T/\psi_{\text{nn}} = 1.4$ (green), $T/\psi_{\text{nn}} = 2.4$ (orange) and $T/\psi_{\text{nn}} = 3.2$ (red). In the inset, the ratio $R = S(0, 2\pi/\sqrt{3}, q_z)/S(2\pi/3, 2\pi/\sqrt{3}, q_z)$ (small dotted arrow compared to large dashed arrow) is plotted as a function of T .

cation. Instead we concentrate on the temperature region above the phase transition.

A combination of Monte Carlo update methods are employed, including single spin flips, parallel tempering and a worm algorithm based on mapping the nearest-neighbour part of the $\psi_{ij}(z)$ interaction [Eq. 2] onto a loop model on the dual honeycomb lattice²⁹. A typical update step includes $9N$ attempts to flip randomly selected individual spins, 10 calls to the worm algorithm and a parallel tempering step. Clusters are hexagonal in shape and contain $N = 3L^2$ lattice sites, where L is the length of the hexagon edges. Simulations are run using $10^4 - 10^5$ updates, with equal numbers of thermalisation and measurement steps.

The ground state of E_{Coul} [Eq. 2] is 6-fold degenerate, and consists of stripes of $\sigma = 1$ alternating with stripes of $\sigma = -1$ [see Fig 1a]. Stripes can be orientated parallel to either A, B or C bonds [see Fig. 1 for bond labelling] and there is a global symmetry associated with flipping all spins $\sigma \rightarrow -\sigma$. At $T_c/\psi_{\text{nn}} \approx 0.19$, with the nearest-neighbour interaction $\psi_{\text{nn}} \approx 0.18$ in the units of Eq. 1, there is an apparently 1st order phase transition into a domain wall network state, as proposed in Ref. [30] for the Ising model with further neighbour exchange interactions. A detailed study of this phase transition will be the subject of another publication.

For $T > T_c$ we perform simulations to measure the dumbbell structure factor. In the absence of interaction between bilayers, this is given by,

$$S(\mathbf{q}_\perp, q_z) = \sin^2 \frac{q_z}{2} \left| \sum_i \sigma_i \exp[i \mathbf{q}_\perp \cdot \mathbf{r}_{\perp,i}] \right|^2, \quad (3)$$

where $\mathbf{r}_{\perp,i}$ measures the position of dumbbell i in the plane of the triangular lattice. Here $q_z = 2\pi z l/c$, where

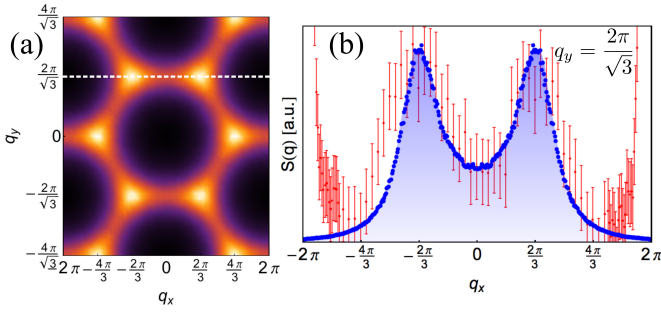


FIG. 3: Comparison between the simulated structure factor following from E_{Coul} [Eq. 1] and x-ray diffraction experiments for $\text{Ba}_3\text{CuSb}_2\text{O}_9$ ⁷. The simulation temperature, T_{frz} , is chosen so as to give the best fit to the experimental data and $L = 48$. (a) Simulated structure factor at $T = T_{\text{frz}}$ with $q_z = \pi$. (b) Cut through the simulated structure factor at $q_y = \frac{2\pi}{\sqrt{3}}$ and $q_z = \pi$ (blue dots, shown by white dashed line in (a)) compared to x-ray diffraction experiments (red dots). Bragg peaks at $q_x = \pm 2\pi$ are ignored in the simulation, since these are independent of the dumbbell ordering.

for $\text{Ba}_3\text{CuSb}_2\text{O}_9$ the dumbbell height is $z = 2.69\text{\AA}$, the unit cell has a height $c = 14.37\text{\AA}$ and l is measured relative to the structural Bragg peaks. For $l = 0$ it is not possible to observe x-ray scattering from the dumbbell structure, as there is a destructive interference between X and Sb ions within the same dumbbell. The signal is strongest when $q_z = (2n + 1)\pi$, where n is an integer, and for $n = 0$ this corresponds to $l = c/(2z) \approx 3$. Fig. 2 shows $S(q_x, 2\pi/\sqrt{3}, \pi)$ at a range of temperatures. Diffuse peaks are centred on $\mathbf{q}_\perp = (\pm 2\pi/3, 2\pi/\sqrt{3})$ [see also Fig. 3a].

The motivation for studying the dumbbell structure factor is that it can be compared with low temperature x-ray diffraction data. This allows the freezing temperature, T_{frz} , of the sample to be determined, and then simulation at this temperature can be used to shed light on the low-temperature structure of the dumbbells in the material. One way to determine T_{frz} is to consider the ratio $R = S(0, 2\pi/\sqrt{3}, q_z)/S(2\pi/3, 2\pi/\sqrt{3}, q_z)$, since this is sensitive to temperature, as can be seen in Fig. 2. The inset to Fig. 2 shows how R increases as a function of T , eventually saturating in the uncorrelated, high-temperature region.

X-ray diffraction data for $\text{Ba}_3\text{CuSb}_2\text{O}_9$, which is taken from Ref. [7], is shown in Fig. 3. The value $R \approx 0.4$ is extracted, giving $T_{\text{frz}}/\psi_{\text{nn}} \approx 0.9$, and the simulated structure factor at this temperature is superposed on the experimental data, showing a good fit. The freezing temperature can be converted into Kelvin by reintroducing the dimensionful prefactors in E_{Coul} [Eq. 1]. The only unknown is the relative permittivity ϵ_r . The dumbbells are definitely frozen at $T = 300\text{K}$, the synthesis temperature is $> 1000\text{K}$ ⁷, and, for T_{frz} to be within these limits, a not unreasonable value of $\epsilon_r \sim 10$ is necessary. Furthermore, the relatively high value of T_{frz} provides a justification for ignoring coupling between bilayers. However, the fact that diffuse scattering is observed at $l = 10$

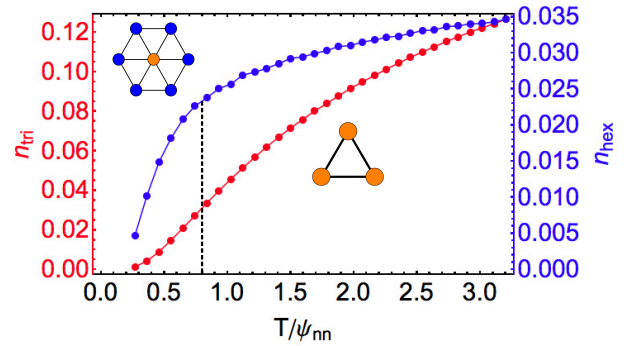


FIG. 4: Fraction of hexagonal plaquettes, n_{hex} , and defect triangles, n_{tri} , as predicted from simulations of E_{Coul} [Eq. 1]. Hexagonal plaquettes are defined as having 6 dumbbells of equivalent orientation surrounding a dumbbell of the opposite orientation. The fraction of hexagonal plaquettes relative to a long range honeycomb lattice ($N/3$ plaquettes) rapidly saturates with increasing temperature at only $n_{\text{hex}} \approx 0.035$ (blue, upper curve). Defect triangles are those in which all three dumbbells have the same orientation, and the fraction relative to a ferromagnetic state ($2N$ defect triangles) steadily increases with temperature (red, lower curve). The black dashed line shows $T/\psi_{\text{nn}} = 0.9$, which is believed to describe the low-temperature dumbbell structure of the $\text{Ba}_3\text{CuSb}_2\text{O}_9$ crystals studied in Ref. [7] (see Fig. 3).

suggests that some correlation is present⁷. This is left for future investigation.

Once T_{frz} has been determined, the dumbbell structure at this effective lattice temperature can be studied in detail. The density of defect triangles, n_{tri} , on which all three dumbbells are orientated in the same direction, is shown in Fig. 4. This density is measured relative to a ferromagnetic state, in which all dumbbells are orientated in the same direction. The density, n_{tri} , increases steadily with temperature and, for $T_{\text{frz}}/\psi_{\text{nn}} = 0.9$, is given by $n_{\text{tri}} \approx 0.03$.

Also shown in Fig. 4 is the density of hexagonal plaquettes, n_{hex} , measured relative to a long-range honeycomb arrangement of dumbbells ($N/3$ plaquettes). Hexagonal plaquettes are defined as 6 equivalently orientated dumbbells surrounding a dumbbell of the opposite orientation. The hexagon plaquette density remains low at all temperatures, rapidly saturating at only $n_{\text{hex}} \approx 0.035$, and, for $T_{\text{frz}}/\psi_{\text{nn}} = 0.9$, is given by $n_{\text{hex}} \approx 0.025$. In Ref. [7], the presence of diffuse peaks in the x-ray diffraction spectrum at $\mathbf{q}_\perp = (2\pi/3, 2\pi/\sqrt{3})$ [see Fig. 3] was taken as proof of a short-range honeycomb arrangement of the dumbbells, since this is the wavevector at which Bragg peaks are found for a long-range ordered honeycomb arrangement. Here we have shown that such a signal arises even in the absence of a significant number of hexagonal plaquettes, the building blocks of the honeycomb lattice.

How should the lattice of X ions be described, if not by a honeycomb lattice? To answer this a representative snapshot of the simulations at $T_{\text{frz}}/\psi_{\text{nn}} = 0.9$ is shown in Fig. 1b. The lattice can be divided into a set of equally orientated clusters – that is clusters of neighbouring dumbbells of the same orientation that are com-

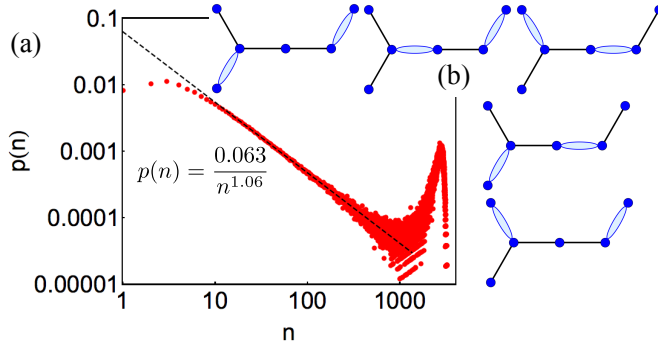


FIG. 5: Statistics of superexchange linked Cu^{2+} clusters at $T_{\text{frz}}/\psi_{\text{nn}} = 0.9$, measured by simulation of E_{Coul} [Eq. 1]. (a) The probability, $p(n)$, that a site belongs to a cluster of size n , calculated using a system of linear size $L = 48$. For $10 < n < 1000$ a power-law distribution $p(n) = 0.063/n^{1.06}$ provides a good fit to the data. At large cluster sizes ($n > 1000$) the finite size of the simulation becomes important. (b) A 6-site superexchange linked cluster of Cu^{2+} ions, with 5 distinct maximal dimer coverings. For geometric reasons, only 4 sites can be covered, leaving 2 monomers (orphan sites).

pletely surrounded by dumbbells of the opposite orientation (shown joined by either blue or orange bonds in Fig. 1b). Superexchange between the electronic degrees of freedom associated with the X ions predominantly occurs within these equally orientated clusters, as superexchange between ions on different monolayers of the same bilayer is expected to be weak⁷. These superexchange-linked clusters can be seen to have a branching structure, and a wide distribution of sizes, n . In Fig. 5 we show $p(n)$, the probability that a given site is part of an n -site cluster. For $L = 48$ ($N=6912$) and for $10 < n < 1000$ a good fit to the numerical data is obtained using a power-law probability function, $p(n) = 0.063/n^{1.06}$. Finite size effects result in a peak of $p(n)$ at large n , and the majority of spins reside in clusters that span the system. While only 19% of sites belong to clusters with $n < 100$, 63% belong to clusters with $n > 2000$. The average cluster size diverges with the size of the system.

It is common in the $\text{Ba}_3\text{XSb}_2\text{O}_9$ family that a sizeable fraction of the electronic spins are “orphaned” and interact only weakly with the rest of the system. This is observed from a variety of experimental probes and, for $\text{X}=\text{Cu}$, the percentage of orphan spins has been measured in the range 5-16%^{6-8,14}. Neutron scattering studies provide evidence that the Cu spins form nearest-neighbour singlet bonds at low temperature⁷, leading us to consider covering the lattice in singlet dimers. Maximally covering the lattice of Cu^{2+} ions with nearest-neighbour singlet dimers leaves a number of orphan spins, due to the geometry of the clusters, and an example of this is shown in Fig. 5b. At $T_{\text{frz}}/\psi_{\text{nn}} = 0.9$ the percentage of orphan spins calculated in this way is 6%, and, for $T > T_c$ this is almost independent of the simulation temperature.

In this dimer picture, clusters with $n = 1$ are guaranteed to be an orphan spin, and make up about 15% of the total orphan spin population. At low tempera-

ture, ESR measures the local environment of the orphan spins⁷, and is therefore biased towards a hexagonal local environment.

It is interesting to speculate as to the low temperature spin-orbital state one may expect in $\text{Ba}_3\text{CuSb}_2\text{O}_9$. Theory suggests that a nearest-neighbour singlet bond is associated with a ferro-orbital alignment between the two sites^{10,12,15}. In order for an orbital resonance to occur, it is therefore necessary for the system to resonate between different singlet coverings of the lattice. The mechanism for this resonance can arise directly from the superexchange interaction, or from coupling to the lattice^{10,12,15}.

For a typical Cu^{2+} superexchange-linked cluster found from solving E_{Coul} [Eq. 1] at $T = T_{\text{frz}}$, there are many possible maximal dimer coverings, which, for geometrical reasons, leave a number of uncovered monomer sites (orphan spins). An oscillation between different dimer coverings can equivalently be viewed as a hopping of orphan spins around the cluster. Thus resonance between different dimer configurations of a cluster not only provides a mechanism by which orbitals can resonate, but also suggests that most orphan spins will be delocalised. In this scenario the dumbbell disorder promotes the creation of a spin-orbital liquid state, which would not necessarily be realised if the dumbbells ordered to form a triangular or honeycomb lattice of Cu ions¹². It would be interesting to explore this scenario of spin-liquid behaviour arising from correlated lattice disorder in more detail.

It is feasible to check experimentally the premise of this article: that X^{2+} - Sb^{5+} dumbbells are flippable at high temperature, freeze as temperature is lowered and that the low-temperature structure can be understood from simulating E_{Coul} [Eq. 1] at T_{frz} . Since T_{frz} is controlled by the cooling rate, there should be a large difference in the dumbbell structure between a crystal slowly cooled from the synthesis temperature and one that is quenched, and this can be studied by making x-ray diffraction measurements and extracting the ratio R (see Fig. 2).

It also may be possible to exert control over the dumbbell structure by applying an electric field during the synthesis process. For example, if a large enough field is applied, it may be possible to access the analogue of the 1/3 magnetisation plateau in Ising systems³¹, in which on every triangle two dumbbells are aligned with the field and one is antialigned. This could lead to a long-range ordered honeycomb lattice of Cu ions.

In conclusion, we have considered the lattice structure of the $\text{Ba}_3\text{XSb}_2\text{O}_9$ family, which includes a number of proposed spin-liquid materials. By studying a model of charged dumbbells on the triangular lattice using Monte Carlo simulations, we find a non-trivial lattice structure [see Fig. 1b], in which superexchange linked clusters of X ions form a branching structure. Focusing in particular on $\text{X}=\text{Cu}$, which has been proposed as a spin-orbital liquid, we show that the obtained lattice structure is consistent with x-ray diffraction data. A simple model of nearest-neighbour singlet covering of the lattice results

in a reasonable estimate for the number of orphan spins, and gives rise to a scenario in which correlated dumbbell disorder promotes a spin-orbital resonant state with non-localised orphan spins.

Acknowledgments. We thank Sergey Korshunov for very useful discussions at the beginning of this work. We also thank Luis Seabra, Ludovic Jaubert and Nic

Shannon for advice on Monte Carlo simulation. We are grateful to Satoru Nakatsuji, Hiroshi Sawa and Naoyuki Katayama for discussions and for sharing their x-ray diffraction data. We thank the Swiss National Science Foundation and its SINERGIA network “Mott physics beyond the Heisenberg model” for financial support.

¹ C. Lacroix, P. Mendels, and F. Mila, *Introduction to Frustrated Magnetism* (Springer, 2011).

² S. Ishihara, M. Yamanaka, and N. Nagaosa, *Phys. Rev. B* **56**, 686 (1997).

³ G. Khaliullin and S. Maekawa, *Phys. Rev. Lett.* **85**, 3950 (2000).

⁴ D. I. Khomskii and M. V. Mostovoy, *Journal of Physics A: Mathematical and General* **36**, 9197 (2003).

⁵ P. Corboz, M. Lajkó, A. M. Läuchli, K. Penc, and F. Mila, *Phys. Rev. X* **2**, 041013 (2012).

⁶ H. D. Zhou, E. S. Choi, G. Li, L. Balicas, C. R. Wiebe, Y. Qiu, J. R. D. Copley, and J. S. Gardner, *Phys. Rev. Lett.* **106**, 147204 (2011).

⁷ S. Nakatsuji, K. Kuga, K. Kimura, R. Satake, N. Katayama, E. Nishibori, H. Sawa, R. Ishii, M. Hagiwara, F. Bridges, T. U. Ito, W. Higemoto, Y. Karaki, M. Halim, A. A. Nugroho, J. A. Rodriguez-Rivera, M. A. Green, and C. Broholm, *Science* **336**, 559 (2012).

⁸ J. A. Quilliam, F. Bert, E. Kermarrec, C. Payen, C. Guillot-Deudon, P. Bonville, C. Baines, H. Luetkens, and P. Mendels, *Phys. Rev. Lett.* **109**, 117203 (2012).

⁹ Y. Ishiguro, K. Kimura, S. Nakatsuji, S. Tsutsui, A. Q. R. Baron, T. Kimura, and Y. Wakabayashi, *Nat Commun* **4** (2013).

¹⁰ J. Nasu and S. Ishihara, *Phys. Rev. B* **88**, 094408 (2013).

¹¹ N. Katayama, K. Kimura, Y. Han, J. Nasu, N. Drichko, Y. Nakanishi, M. Halim, Y. Ishiguro, R. Satake, E. Nishibori, M. Yoshizawa, T. Nakano, Y. Nozue, Y. Wakabayashi, S. Ishihara, M. Hagiwara, H. Sawa, and S. Nakatsuji, [arXiv:1403.4779 \[cond-mat.str-el\]](https://arxiv.org/abs/1403.4779).

¹² A. Smerald and F. Mila, *Phys. Rev. B* **90**, 094422 (2014).

¹³ K. V. Shanavas, Z. S. Popović, and S. Satpathy, *Phys. Rev. B* **89**, 085130 (2014).

¹⁴ S.-H. Do, J. van Tol, H. D. Zhou, and K.-Y. Choi, *Phys. Rev. B* **90**, 104426 (2014).

¹⁵ J. Nasu and S. Ishihara, *Phys. Rev. B* **91**, 045117 (2015).

¹⁶ J. G. Cheng, G. Li, L. Balicas, J. S. Zhou, J. B. Goodenough, C. Xu, and H. D. Zhou, *Phys. Rev. Lett.* **107**, 197204 (2011).

¹⁷ C. Xu, F. Wang, Y. Qi, L. Balents, and M. P. A. Fisher, *Phys. Rev. Lett.* **108**, 087204 (2012).

¹⁸ S. Bieri, M. Serbyn, T. Senthil, and P. A. Lee, *Phys. Rev. B* **86**, 224409 (2012).

¹⁹ G. Chen, M. Hermele, and L. Radzihovsky, *Phys. Rev. Lett.* **109**, 016402 (2012).

²⁰ K. Hwang, T. Dodds, S. Bhattacharjee, and Y. B. Kim, *Phys. Rev. B* **87**, 235103 (2013).

²¹ Y. Shirata, H. Tanaka, A. Matsuo, and K. Kindo, *Phys. Rev. Lett.* **108**, 057205 (2012).

²² T. Susuki, N. Kurita, T. Tanaka, H. Nojiri, A. Matsuo, K. Kindo, and H. Tanaka, *Phys. Rev. Lett.* **110**, 267201 (2013).

²³ G. Koutroulakis, T. Zhou, Y. Kamiya, J. D. Thompson, H. D. Zhou, C. D. Batista, and S. E. Brown, *Phys. Rev. B* **91**, 024410 (2015).

²⁴ Z. Tian, C. Zhu, Z. Ouyang, J. Wang, W. Tong, Y. Liu, Z. Xia, and S. Yuan, *Journal of Magnetism and Magnetic Materials* **360**, 10 (2014).

²⁵ Z. Tian, Q. Guo, Z. Ouyang, G. Du, W. Tong, J. Wang, and S. Yuan, *Solid State Communications* **191**, 66 (2014).

²⁶ T. Dey, A. V. Mahajan, P. Khuntia, M. Baenitz, B. Koteswararao, and F. C. Chou, *Phys. Rev. B* **86**, 140405 (2012).

²⁷ A. Grzybowski, E. Gwóźdź, and A. Bródka, *Phys. Rev. B* **61**, 6706 (2000).

²⁸ U. K. Rößler, *Journal of Applied Physics* **89**, 7033 (2001).

²⁹ W. Zhang, T. M. Garoni, and Y. Deng, *Nuclear Physics B* **814**, 461 (2009).

³⁰ S. E. Korshunov, *Phys. Rev. B* **72**, 144417 (2005).

³¹ B. Nienhuis, H. J. Hilhorst, and H. W. J. Blote, *Journal of Physics A: Mathematical and General* **17**, 3559 (1984).